Research Square

Preprints are preliminary reports that have not undergone peer review.
They should not be considered conclusive, used to inform clinical practice,
or referenced by the media as validated information.

Targeting LCN2 attenuates abnormal lymphatic remodeling and SiO_2 induced pulmonary fibrosis

Yue Zhang

158408366920163.com

North China University of Science and Technology School of Public Health https://orcid.org/0009-0006-1102-0869

Fangze Wan

North China University of Science and Technology School of Public Health

Xinyao Wang

North China University of Science and Technology School of Public Health

Yuexi Xie

North China University of Science and Technology School of Public Health

Heliang Liu

North China University of Science and Technology School of Public Health

Hailan He

North China University of Science and Technology School of Public Health https://orcid.org/0000-0002-3521-1815

Research Article

Keywords: LCN2, SiO2, ZINC00640089, Lymphangiogenesis, Pulmonary fibrosis

Posted Date: September 23rd, 2026

DOI: https://doi.org/10.21203/rs.3.rs-10835546/v1

License: This work is licensed under a Creative Commons Attribution 4.0 International License.
Read Full License

Abstract

Background

Long-term exposure to respirable crystalline free silica (SiO_2) is one of the most common and persistent hazards in occupational environments, leading to silicosis and causing progressive fibrotic lung disease, although its fibrogenic molecular mechanisms have not yet been fully elucidated.

Objective

Objective: This study aims to investigate the role of LCN2 in silica-induced pulmonary fibrosis, with a focus on its regulatory effect on pathological lymphangiogenesis and the underlying molecular mechanisms.

Methods

To investigate the regulatory role of LCN2 in silica-induced lymphangiogenesis and fibrosis, serum levels of LCN2 and VEGF-C were measured by ELISA in 73 silicosis patients and 15 healthy controls. A silicosis mouse model was established by intratracheal instillation of SiO_2, and the effects of the LCN2 inhibitor ZINC00640089 were evaluated by histopathological staining (HE, VG, and Sirius red), micro-CT imaging, and Western blot analysis of fibrosis and lymphangiogenesis-related markers. Additionally, RNA sequencing was performed to identify differentially expressed genes and signaling pathways modulated by ZINC00640089. To further validate the functional role of LCN2 in lymphatic endothelial cells, in vitro scratch assays and Matrigel tube formation assays were conducted using human lymphatic endothelial cells (HLECs).

Results

Serum LCN2 and VEGF-C were significantly elevated in silicosis patients. In the silicosis mouse model, ZINC00640089 attenuated pulmonary fibrosis and inflammatory infiltration, accompanied by downregulation of VEGF-C, VEGFR-3, and LYVE-1. Transcriptomic analysis revealed that ZINC00640089 modulated pathways related to inflammation and lymphangiogenesis, including VEGF signaling. Immunofluorescence confirmed LCN2 colocalization with LYVE-1 in lung tissues. In vitro, ZINC00640089 suppressed SiO_2-induced HLEC migration and tube formation.

Conclusion

This study demonstrates that targeting LCN2 can prevent abnormal lymphatic remodeling and alleviate SiO_2-induced pulmonary fibrosis, providing a promising therapeutic strategy for silicosis.

1. Introduction

Silicosis is the most prevalent and harmful type of pneumoconiosis. It is a progressive and irreversible systemic disease characterized by diffuse pulmonary fibrosis, caused by long-term inhalation of free silicon dioxide (SiO_2)[1]. The pathogenesis of silicosis is complex, and requires further research to develop effective treatment methods. Therefore, the search for new intervention targets and prevention methods is one of the hotspots and focuses in the research field of silicosis prevention and treatment.

The lymphatic system is an important systemic circulatory system within the body, functioning to remove large molecules from the interstitial fluid and maintaining the balance of the internal environment of tissues[2]. Lymphatic vessels are an important part of the lymphatic system. They assist in immune surveillance, returning exuded interstitial fluid to the bloodstream, and absorbing dietary lipids from the intestine, thereby maintaining the balance of the interstitial environment[3]. Studies have shown that the SiO_2 inhaled into the lungs can be drained out of the body through the lymphatic vessels within the lungs, reducing the silicon content in the lung tissue[4]. This indicates that the pulmonary lymphatic circulation may play a significant role in the progression of silicosis.

Lipocalin-2 (LCN2) is a secreted innate immune protein that can promote pulmonary fibrosis through the STAT3-TGF-β1-Smad3 signaling pathway[5]. In addition to serving as a biomarker, LCN2 can also act as a secreted signaling molecule. It can promote the proliferation and lumen formation of lymphatic endothelial cells (LEC) by activating the PI3K-VEGFC-VEGFR-3 signaling axis, thereby driving pathological lymphangiogenesis[6]. Previous studies have confirmed that the VEGFC/VEGFR3 pathway can regulate the lymphatic vessel formation in silicosis, thereby influencing the progression of silicosis fibrosis[7]. It is suggested that LCN2 may play a significant role in the process of lymphatic vessel formation in silicosis. ZINC00640089 is a selective small molecule antagonist targeting LCN2. It initially demonstrated the ability to inhibit tumor cell proliferation and reduce Akt phosphorylation levels in an inflammatory breast cancer model[8]. It is worth noting that recent in vivo studies have expanded its application scope beyond the oncology field, demonstrating that in a mouse model of renal ischemia-reperfusion injury, pharmacological LCN2 inhibition using ZINC00640089 can alleviate ferroptosis and tissue damage[9]. This suggests that targeted inhibition of LCN2 and its-mediated pathological lymphangiogenesis becomes an important intervention strategy for blocking the fibrotic process of silicosis. We speculate that ZINC00640089 may affect the progression of silicosis by blocking LCN2 and remodeling the structure and function of pulmonary lymph circulation.

Therefore, this study employs ZINC00640089 as a pharmacological tool to investigate the regulatory role of LCN2 inhibition on lymphatic vessel formation in silicosis and its impact on pulmonary fibrosis, providing new targets and experimental evidence for the clinical prevention and treatment of silicosis.

2. Materials and methods

2.1 Population sample selection

This study selected 73 male patients with silicosis who underwent large-volume whole lung lavage for the first time at the Beidaihe Rehabilitation Hospital of the Ministry of Emergency Management in 2022. 15 healthy males were used as serum controls. The patients' diagnoses were based on "Diagnosis of Occupational Pneumoconiosis" (GBZ70–2015), and patients with infectious diseases, abnormal liver function, hyperlipidemia, and those with active pulmonary diseases such as pneumonia were excluded. The research protocol was approved by the Medical Ethics Committee of North China University of Science and Technology (2021041), and all participants signed informed consent forms.

2.2 Animal grouping and treatment

Male SPF-grade C57BL/6 mice (SCXK 2020-0001, Liaoning, China), 6–8 weeks old and weighing 16–18 g, were purchased from Liaoning Changsheng Biotechnology Co., Ltd. The mice were housed in a barrier facility at the Experimental Animal Center of North China University of Technology under controlled conditions: constant temperature (22 ± 2°C), humidity (50%–60%), and a 12-hour light-dark cycle, with ad libitum access to food and water. All experimental procedures were approved by the Animal Ethics Committee of North China University of Technology (2025322) and conducted in accordance with animal welfare guidelines. After one week of acclimation, C57BL/6 mice were randomly divided into four groups: (1) Control group (n = 8): mice received a single tracheal instillation of 50 μL 0.9% saline, followed by intraperitoneal injections of 100 μL 0.9% saline every other day for 4 weeks; (2) ZINC00640089 group (n = 8): mice received a single tracheal instillation of 50 μL 0.9% saline, followed by intraperitoneal injections of 100 μL 2 mg/mL ZINC00640089 (10 mg/kg) every other day until the end of week 4; (3) Silicosis group (n = 8): mice received a single tracheal instillation of 100 mg/mL SiO_2 suspension[10] (Sigma, USA), followed by intraperitoneal injections of 100 μL 0.9% saline every other day until week 4; (4) Silicosis+ZINC00640089 group (n = 8): mice received a single tracheal instillation of 100 mg/mL SiO_2 suspension, followed by intraperitoneal injections of 100 μL 2 mg/mL ZINC00640089 every other day until week 4. At the end of week 4, blood was collected via orbital puncture, plasma was separated and stored at − 80°C. The left lung was fixed in 4% paraformaldehyde for histopathological staining, while the remaining lung tissue was rapidly frozen in liquid nitrogen and stored at − 80°C.

2.3 Cell culture and treatment

Human lymphatic endothelial cells (HLECs) were obtained from Science Cell (USA). The cells were cultured in complete ECM medium (Gibco, USA) supplemented with 10% fetal bovine serum, under the conditions of 37°C and 5% CO_2 in a cell incubator. The cells were then divided into four groups: (1) Control group; (2) ZINC00640089 group: treated with 2 μg/mL ZINC00640089 for 24 hours; (3) SiO_2 group: treated with 50 μg/mL SiO_2 for 36 hours; (4) SiO_2+ZINC00640089 group: first treated with 50 μg/mL SiO_2 for 36 hours, and at the 12-hour mark, further treated with 2 μg/mL ZINC00640089 for 24 hours.

2.4 Enzyme-linked immunosorbent assay (ELISA)

Peripheral venous blood samples were collected from 73 silicosis patients and 15 healthy controls. After clotting at room temperature for 30 minutes, the serum was separated by centrifugation at 3000 rpm for

15 minutes and stored at -80°C. Serum concentrations of LCN2 and vascular endothelial growth factor C (VEGF-C) were quantified using ELISA kits (Abclonal Company, USA) according to the manufacturer's instructions. Absorbance values were measured at a wavelength of 450 nm using a microplate reader.

2.5 RNA sequencing

Mice were euthanized after 4 weeks of feeding, and appropriate amounts of lung tissue were collected and stored in liquid nitrogen. RNA sequencing of the lung tissues was perfomed by Guangke Ande Biotechnology Co., Ltd. in Hangzhou, China. Differentially expressed genes (DEGs) were identified between the Control group and Silicosis group, as well as between the Silicosis group and the Silicosis+ZINC00640089 group. Genes with a *P*-value < 0.05 and Fold Change > 2 were selected as screening criteria to identify differentially expressed genes in mouse lung tissues, followed by GO enrichment and KEGG pathway analysis.

2.6 Micro computed tomography

After inducing inhalation anesthesia in mice with isoflurane (Ante Animal Husbandry, Jinan, China), in vivo mouse lung computed tomography images were obtained using the NEMO-II NMC-20 micro-CT scanner (Pingsheng, Jiangsu, China). Mice were positioned supine, and data were reconstructed offline using the recon software, while the avatar software was used to acquire and analyze the data.

2.7 Hematoxylin and Eosin Staining

After fixation, dehydration, and paraffin embedding of lung tissue, 5 μm sections were cut. The sections were baked at 60°C, dewaxed and hydrated with xylene and graded ethanol, then stained with hematoxylin for 5 minutes. After differentiation with 2% alcohol acid and bluing under running water, they were counterstained with eosin for 1 minute. Subsequently, the sections were dehydrated through graded ethanol, cleared with xylene, and mounted with neutral gum. Histopathological changes in the lung tissue were observed under a microscope.

2.8 VG staining

After the lung tissue underwent fixation, dehydration, paraffin embedding, and sectioning as described above, it was stained using a picric acid acid fuchsin staining kit (VG, Solarbio, China) to assess collagen deposition in the lung tissue. The stained samples were examined and imaged under an Olympus DP80 optical microscope.

2.9 Western blot

Proteins were extracted from lung tissues and cells of different experimental groups, and factors related to lymphangiogenesis, inflammation, and fibrosis were detected by Western blot. The primary antibodies used in this study included: β-Actin (1:10000, Abclonal, USA), COL Ⅰ(1:1000, HuaAn Biotechnology, China), Lipocalin-2 (1:1000, Affinity, USA), FN (1:1000, HuaAn Biotechnology, China), VEGFR-3 (1:1000, HuaAn Biotechnology, China), Eca (1:1000, GeneTex, USA), VEGF-C (1:1000, HuaAn Biotechnology, China), LYVE-1 (1:1000, HuaAn Biotechnology, China), IL-1β (1:1000, Ruipate, China), and IL-6 (1:1000,

Ruipate, China). The secondary antibodies were anti rabbit (1:5000, Cell Signaling, USA) and anti-mouse (1:5000, Seracare, USA).

2.10 Immunohistochemical

After dewaxing and hydration of the paraffin sections, they were subjected to high-pressure heat repair using sodium citrate buffer. The endogenous peroxidase was inactivated with 3% H_2O_2, and non-specific sites were blocked with 3% BSA. One-antibody LCN2 (1:50) and LYVE-1 (1:100) were dropped onto the sections and incubated at 4°C in a humid box overnight. The next day, HRP-labeled secondary antibody (1:200) was added and incubated at 37°C for 30 minutes. DAB staining was performed, followed by hematoxylin re-staining. The sections were dehydrated, transparentified, and sealed with neutral gum. Images were collected using an optical microscope.

2.11 Immunofluorescence

As described above, after dewaxing and rehydration of paraffin sections, antigen retrieval was performed using sodium citrate buffer under high-pressure heat treatment. Endogenous peroxidase activity was blocked with 3% hydrogen peroxide, followed by incubation with 3% BSA at room temperature for blocking. Primary antibody mixture (LCN2, 1:50; LYVE-1, 1:100) and α-SMA (1:50) were separately applied and incubated overnight at 4°C in a humidified chamber. The next day, fluorescently labeled secondary antibody (goat anti-rabbit IgG, 1:200) was added and incubated at 37°C in the dark for 90 minutes. After washing with PBS, slides were mounted with DAPI containing anti-fade mounting medium, then observed and imaged under a fluorescence microscope.

2.12 Cell scratch assay

Cells were seeded into a 6-well plate until reaching 90% confluence, and a scratch was made vertically across the bottom of the plate using a sterile 200 μL pipette tip. The cells were washed three times with PBS to remove floating cells, then the medium was replaced with fresh medium containing 2% FBS. Images were captured at the same field of view at 0 h and 24 h. Cell migration rate was calculated using Image J software: migration rate (%) = (scratch area at 0 h - scratch area at 24 h) / scratch area at 0 h × 100%.

2.13 Tube formation assay

Pre-coat 24-well plates with Matrigel (Mogengel, Xiamen, China) and allow polymerization at 37°C for 45 minutes. Subsequently, seed HLECs cell suspension and continue culturing in a 37°C, 5% CO_2 incubator. Observe and photograph tube-like structures under an inverted microscope at 0 h and 24 h, and quantitatively analyze parameters such as the number of tubes formed, coverage area, and branch points using Image J software.

2.14 Statistical analysis

Experimental data were analyzed using SPSS 23.0 statistical software, with all data expressed as mean ± standard deviation. For comparisons between two groups, independent samples t-tests were used; for

multiple group comparisons, one-way analysis of variance based on a completely randomized design was applied. Pairwise comparisons were conducted using the least significant difference test when variances were homogeneous, and Tamhane's T2 test was used when variances were heterogeneous. Differences were considered statistically significant at $P < 0.05$.

3. Results

3.1 Elevated serum levels of LCN2 and VEGF-C in patients with silicosis

This study included a population sample of male silicosis patients and healthy controls from the Beidaihe Rehabilitation Hospital of the Ministry of Emergency Management. ELISA results showed that, compared with the healthy control group, LCN2 and the lymphatic endothelial marker VEGF-C were significantly elevated in silicosis patients (Fig. 1A-B).

3.2 ZINC00640089 targets LCN2 to ameliorate fibrosis in silica-exposed mice

To investigate the therapeutic potential of targeting LCN2 in silicosis, we established a treatment protocol as shown in Fig. 2A. HE staining (Fig. 2B) revealed that lung tissue architecture was clear and intact in both the Control and ZINC00640089 groups; however, in the Silicosis group, alveolar structures were severely damaged with inflammatory cell infiltration, and some alveolar spaces were reduced or absent. In contrast, the Silicosis+ZINC00640089 group showed significantly less lung tissue damage compared to the Silicosis group, with smaller nodules. VG staining (Fig. 2C) and Sirius red staining (Fig. 2D) further confirmed that interstitial collagen fibers were markedly increased in the Silicosis group, appearing as linear or patchy deposits, indicating obvious pulmonary fibrosis. After ZINC00640089 intervention, collagen fiber deposition was significantly reduced, and the degree of interstitial fibrosis was alleviated. Additionally, Western blot analysis showed upregulated expression of IL-1β, LCN2, COL I, and FN, and downregulated expression of Eca in lung tissues of the Silicosis group. Following ZINC00640089 treatment, levels of IL-1β, LCN2, COL I, and FN were decreased, while Eca expression was increased in the Silicosis group (Figs. 2E–J). Micro-CT revealed clear lung textures and no abnormal density shadows in the Control and ZINC00640089 groups (Fig. 3A). In contrast, the Silicosis group showed thickened lung textures and high-density shadows within the lung fields. However, after treatment with ZINC00640089, both the extent and density of these high-density shadows were significantly reduced. Additionally, immunofluorescence results indicated that (Fig. 3B), compared to the Control and ZINC00640089 groups, α-SMA green fluorescent signals were significantly enhanced in the lung tissues of the Silicosis group. Treatment with ZINC00640089 markedly weakened the intensity of α-SMA fluorescence signals.

3.3 Transcriptome analysis reveals that ZINC00640089 regulates signaling pathways associated with silica-induced lung inflammation and lymphatic vessel formation

To elucidate the molecular mechanisms by which ZINC00640089 regulates the progression of silicosis, we performed RNA-seq transcriptome analysis on lung tissues from the Control group, Silicosis group, and Silicosis+ZINC00640089 group. Differentially expressed genes (DEGs) were identified using criteria of Fold Change > 2 and *P*-value < 0.05. Compared to the Control group, the Silicosis group showed significant differential expression in 3166 genes (Fig. 4A-B), including 1984 upregulated and 1182 downregulated genes. GO and KEGG enrichment analyses revealed that these DEGs were primarily enriched in pathways such as mesenchymal to epithelial transition, cell chemotaxis, regulation of inflammatory response, immune response-regulating signaling pathway, and lymphocyte migration (Fig. 4C-F). In comparison between the Silicosis and Silicosis+ZINC00640089 groups, a total of 544 genes exhibited significant differential expression (Fig. 4G-H), with 265 upregulated and 279 downregulated genes. The DEGs were mainly enriched in pathways including ECM-receptor interaction, regulation of inflammatory response, regulation of endothelial cell chemotaxis, and regulation of blood vessel endothelial cell proliferation involved in sprouting angiogenesis (Fig. 4I-L). Furthermore, we performed a venn diagram analysis comparing the DEGs in the Control and Silicosis groups with those in the Silicosis and Silicosis+ZINC00640089 groups, identifying 197 overlapping DEGs (Fig. 5A). KEGG analysis revealed that genes upregulated in the Silicosis group but downregulated in the Silicosis+ZINC00640089 group were primarily enriched in signaling pathways such as cytokine-cytokine receptor interaction, chemokine signaling pathway, VEGF signaling pathway, and IL-17 signaling pathway. Conversely, genes downregulated in the Silicosis group but upregulated in the Silicosis+ZINC00640089 group were mainly enriched in ECM-receptor interaction, platelet activation, and MAPK signaling pathway (Figs. 5B-C).

3.4 Inhibition of LCN2 can block pathological lymphatic vessel formation

To investigate the regulatory role of LCN2 in lymphangiogenesis in silicosis, we first examined the relationship between LCN2 and lymphatic vessel formation using immunofluorescence colocalization (Fig. 6A). Compared with the Control group, both LCN2 and the lymphatic endothelial marker LYVE-1 showed enhanced fluorescent signals in the Silicosis group, with significantly increased colocalized areas. However, after intervention with ZINC00640089, the fluorescent signals for both LCN2 and LYVE-1 were markedly reduced, and their overlap decreased. Immunohistochemical staining (Fig. 6B) revealed that, compared to the Control group, the Silicosis group exhibited damaged alveolar structures, along with significantly elevated expression of LCN2 and LYVE-1 in lung tissues; following ZINC00640089 treatment, the expression levels of both LCN2 and LYVE-1 were substantially downregulated. To further validate the regulatory effect of LCN2 on lymphangiogenesis, we analyzed the expression of relevant marker proteins by Western blot (Figs. 6C–F). In the Silicosis group, the expression of VEGF-C, VEGFR-3, and LYVE-1 was upregulated; however, targeted inhibition of LCN2 effectively reversed this trend.

3.5 Targeted inhibition of LCN2 alleviates SiO_2-induced alterations in lymphatic function of HLECs

To clarify the role of LCN2 in SiO_2-induced lymphatic endothelial cell migration and tube formation, we first determined the cytotoxicity of the LCN2 inhibitor ZINC00640089 on HLECs across a concentration range of 0–20 μM. Based on its dose dependent effect (Fig. 7A), 10 μM was selected as the concentration for all subsequent treatments. Scratch assay results showed that SiO_2 stimulation for 24 hours significantly increased migration area (Fig. 7B-C). However, treatment with ZINC00640089 effectively attenuated this effect, resulting in a significant reduction in migration area compared to the SiO_2 group. To further validate the role of targeting LCN2 in regulating HLEC function, we performed Matrigel tube formation assays to assess their angiogenic capacity (Fig. 7D). Results revealed that SiO_2 stimulation induced increased formation of network-like structures. In contrast, cells treated with SiO_2+ZINC00640089 exhibited dispersed morphology and loose intercellular connections. Quantitative analysis showed that, compared to the SiO_2 group, the number of tube-like structures and branch points were significantly reduced in the SiO_2 +ZINC00640089 group (Figs. 7E-F). Additionally, Western blot analysis demonstrated that, compared to the control group, SiO_2 exposure significantly upregulated LYVE-1, VEGF-C/VEGFR-3, FN, IL-6, and IL-1β in HLECs; however, treatment with the LCN2 inhibitor ZINC00640089 downregulated the protein levels of FN, VEGF C, VEGFR-3, LYVE-1, IL-6, and IL-1β (Figs. 7G–N).

4. Discussion

Silicosis, caused by long-term inhalation of respirable dust containing free SiO_2, remains a major public health and social issue affecting public health in China[11]. SiO_2 particles can stimulate alveolar macrophages to secrete VEGF-C, thereby promoting lymphatic vessel formation. Lymphatic drainage impairment and dysregulation of the VEGF-C/VEGFR-3 signaling pathway have been recognized as jointly contributing to inflammation and fibrosis in silicosis[7]. LCN2, a stress-induced secreted apolipoprotein, has been shown to promote fibrosis in kidney disease[12], but its role in lymphatic regulation in silicosis remains unclear. This study demonstrates that intervention with the LCN2 inhibitor ZINC00640089 improves pulmonary inflammation and abnormal lymphatic vessel formation, thereby alleviating the progression of silicotic fibrosis. These findings offer new insights into the pathogenesis of silicosis and provide a potential avenue for developing targeted therapeutic strategies.

This study used clinical samples and a mouse model to validate the effects of targeting LCN2 inhibition. Clinical sample analysis revealed that in the serum of silicosis patients, LCN2 and the key lymphangiogenesis factor VEGF-C simultaneously increased. This is consistent with the reports that LCN2 is upregulated in fibrotic lung diseases[13], suggesting that LCN2 may be associated with lymphatic dysfunction and participate in the pathological process of silicosis. In terms of mechanism verification, after the intervention of the small molecule inhibitor ZINC00640089, the histological staining and Micro-CT results showed that the collagen deposition in the silicosis mouse model was reduced, the

inflammatory infiltration was alleviated, and the pulmonary nodules improved. Immunofluorescence staining for α-SMA showed that SiO_2 exposure significantly induced myofibroblast activation, whereas treatment with ZINC00640089 markedly suppressed this fibrotic process—consistent with prior findings linking LCN2 to fibrosis progression in silicosis[5]. Collectively, the concurrent elevation of LCN2 and VEGF-C in clinical samples suggests their connection to lymphatic dysfunction, while targeted inhibition of LCN2 in the mouse model alleviated myofibroblast activation and interstitial lesions. To further elucidate the underlying molecular mechanisms, we performed transcriptome sequencing.

We analyzed transcriptome sequencing data to explore the mechanistic role of targeting LCN2 in inhibiting pulmonary fibrosis. Differential gene analysis and GO/KEGG enrichment revealed that ZINC00640089 treatment significantly altered the gene expression profile induced by SiO_2 exposure, with differentially expressed genes notably enriched in lymphocyte migration, regulation of endothelial cell chemotaxis, and activation of the NF-κB signaling pathway. These findings are highly consistent with the characteristics of lung inflammation and inflammatory cell infiltration caused by SiO_2 exposure. As a central regulatory hub for pro-inflammatory cytokine transcription, NF-κB suggests that SiO_2 drives the release of numerous cytokines via activation of this classic inflammatory axis[14]. Venn diagram intersection analysis and KEGG network construction revealed that Cytokine-cytokine receptor interaction forms a densely interconnected network with the IL-17 signaling pathway, TNF signaling pathway, and VEGF signaling pathway, indicating that SiO_2 exposure establishes a complex, multi-pathway pro-inflammatory network within lung tissue. Among these, the enriched IL-17 signaling pathway has previously been shown to induce LCN2 expression through the NF-κB/IκBζ axis in conjunction with TNF-α[15]. In our study, LCN2 was significantly upregulated following SiO_2 exposure, and it is known to promote epithelial mesenchymal transition (EMT) and fibrosis via the STAT3-TGF-β1-Smad3 axis, suggesting that LCN2 may serve as a key effector molecule linking inflammatory signals to fibrotic progression[5]. Meanwhile, the enrichment of the VEGF signaling pathway warrants attention. The VEGF C/VEGFR3 axis is a well-established pathway driving proliferation, migration, and lumen formation of lymphatic endothelial cells[16], and abnormal lymphangiogenesis observed in silicosis provides a conduit for persistent immune cell infiltration[7]. Given the significant enrichment of the VEGF signaling pathway in our transcriptome data and its role in promoting lymphatic vessel formation, we hypothesize that LCN2 may also participate in regulating lymphatic endothelial cells. Previous studies have shown that controlled lymphatic regeneration after acute injury can alleviate inflammation[17]. However, other research has demonstrated that sustained SiO_2 deposition in silicosis leads to impaired lymphatic drainage and pathological remodeling of lymphnodes[7]. In the SiO_2 model of this study, we hypothesized that the lymphatic vessel hyperplasia accompanying LCN2 also exhibited a similar trend, being a pathological remodeling rather than a protective regeneration. Therefore, we subsequently verified this through double immunofluorescence staining and in vitro experiments.

Based on transcriptome analysis, we employed dual immunofluorescence staining to validate the colocalization of LCN2 and LYVE-1, and confirmed their regulatory interaction through in vitro experiments. Immunofluorescence results showed that after SiO_2 exposure, the fluorescent signals of

LCN2 overlapped significantly with those of LYVE-1, whereas this signal intensity was markedly reduced following intervention with ZINC00640089. Previous studies from our group have demonstrated that persistent SiO_2 deposition drives pulmonary lymphatic abnormalities[18]. In this study, we found that LCN2 selectively accumulates in these proliferative lymphatic vessels, suggesting its involvement in lymphatic pathophysiology. Existing research has established that LCN2, as a stress responsive secreted protein, participates in tissue injury and remodeling in silicosis[5]. Moreover, lung lymphatic vessels serve not only as drainage pathways but also as microenvironmental regulators governing inflammation resolution and tissue remodeling[17]. Integrating these findings with our current data, we hypothesize that LCN2 may mediate functional regulation of pulmonary lymphatic endothelial cells, and its aberrant expression is closely associated with lymphatic-driven tissue remodeling. We further confirmed in vitro that ZINC00640089 directly inhibits HLEC migration and tube formation, while downregulating VEGF-C and LCN2 protein levels—findings consistent with the improvement in abnormal lymphangiogenesis observed in vivo. In summary, these results suggest that LCN2 may be more than just an inflammatory companion factor; it could represent a key molecular link between lymphatic abnormalities and fibrotic progression.

Currently, pirfenidone and nintedanib, which are clinically used to treat silicosis, often cause severe gastrointestinal side effects that may lead to dose reduction or even discontinuation of treatment[19]. However, toxicological studies have shown that ZINC00640089 did not induce significant liver or kidney damage in mice across various dosage groups, demonstrating overall good tolerability[20]. In this study, ZINC00640089 achieved multiple therapeutic effects—including anti-inflammatory action, inhibition of abnormal lymphatic vessel formation, and reduction of fibrosis—by targeting LCN2. Compared to single-target drugs, this multi-node intervention may hold greater potential in halting the progression of silicosis, providing preliminary evidence for a novel early intervention strategy.

This study still has several limitations: although ZINC00640089 demonstrated promising anti fibrotic and inhibitory effects on lymphatic abnormalities both in vitro and in vivo, the exact binding site to LCN2 remains unclear. The animal model used a single intratracheal instillation of SiO_2 in mice to induce silicosis, which primarily reflects the early inflammatory and fibrotic stages of the disease but does not fully replicate the clinical progression of human silicosis; therefore, further validation is needed using models with greater clinical relevance. In vitro experiments employed a human lymphatic endothelial cell line, which may not fully capture functional differences observed in primary lymphatic endothelial cells. Although the association between LCN2 and lymphatic abnormalities has been established, the specific molecular mechanisms by which LCN2 regulates the VEGF-C/VEGFR3 axis—such as whether it involves direct transcriptional regulation or indirect signaling pathways—remain to be elucidated.

In summary, this study reveals that LCN2 is closely associated with abnormal pulmonary lymphatic vessel formation in silicosis and participates in the fibrotic pathological process. The small molecule ZINC00640089 effectively ameliorates SiO_2-induced lymphatic abnormalities and lung structural damage

by inhibiting LCN2 (Fig. 8). These findings provide new insights into the pathogenesis of silicosis and offer preliminary experimental evidence for developing anti-fibrotic drugs targeting LCN2.

Declarations

Ethics approval and consent to participate

This study was conducted in accordance with the Declaration of Helsinki. The research protocol involving human participants was approved by the Medical Ethics Committee of North China University of Science and Technology (Approval No. 2021041), and all participants provided written informed consent. All animal experiments were approved by the Animal Ethics Committee of North China University of Technology (Approval No. 2025322) and were performed in compliance with the Guide for the Care and Use of Laboratory Animals.

Consent for publication

No human subject images or clinical case data are presented in this manuscript, so additional publication consent is not required.

Competing interests

The authors declare no competing interests.

Funding

This work was supported by National Natural Science Foundation of China (U21A20334, 82606977), Natural Science Foundation of Hebei Province (H2025209083, H2025209038), Higher Education Scientific Research Project of Hebei Province (QN2026045).

Author contributions

H.L. and H.H. designed this study. Y.Z. was in charge of the whole experiment conduction and wrote the manuscript. F.W., X.W. and Y.X. helped to prepare figures and analyze data. All authors reviewed the manuscript.

Availability of data and material

All data supporting the findings of this study are included within the paper and its Supplementary Information files.

References

1. He H, Qi R, Cui J, et al. Lipid characteristics of lung tissue in silicosis rat model were studied based on lipid metabolomics[J]. Toxicol Lett. 2024;391:111–9.
2. Aspelund A, Robciuc MR, Karaman S, et al. Lymphatic System in cardiovascular medici ne[J]. Circ Res. 2016;118(3):515–30.
3. Jakus Z, Hong YK, Kume T, Editorial. Lymphatic system: organ specific functions in hea lth and disease, II[J]. Front Cell Dev Biol. 2025;13:1659266.
4. Yu J, Mao L, Guan L, et al. Ginsenoside Rg1 enhances lymphatic transport of intrapulmo nary silica via VEGF-C/VEGFR-3 signaling in silicotic rats[J]. Biochem Biophys Res Commun. 2016;472(1):182–8.
5. Xie Z, Li X, Zhang M, et al. LCN2-positive alveolar type II cells promote silica-induced pulmonary fibrosis via STAT3-TGF-β1-Smad3-mediated signaling[J]. Toxicol Appl Pharmacol. 2025;505:117579.
6. Jung M, Ören B, Mora J, et al. Lipocalin 2 from macrophages stimulated by tumor cell-derived sphingosine 1-phosphate promotes lymphangiogenesis and tumor metastasis[J]. Sci Signal. 2016;9(434):64.
7. Zhang J, Cui J, Li X, et al. Increased secretion of VEGF-C from SiO_2-induced pulmonary macrophages promotes lymphangiogenesis through the Src/eNOS pathway in silicosis[J]. Ecotoxicol Environ Saf. 2021;218:112257.
8. Santiago-Sánchez GS, Noriega-Rivera R, Hernández-O'Farrill E, et al. Targeting Lipocalin-2 in Inflammatory Breast Cancer Cells with Small Interference RNA and Small Molecule Inhibitors[J]. Int J Mol Sci. 2021;22(16):8581.
9. Wu Z, Yu B, He Q, et al. LCN2 drives ferroptosis-associated ischemia-reperfusion injury after renal transplantation: integrated machine learning and in vivo validation[J]. Apoptosis. 2025;30(11–12):3026–43.
10. Mayeux JM, Kono DH, Pollard KM. Development of experimental silicosis in inbred and outbred mice depends on instillation volume[J]. Sci Rep. 2019;9(1):14190.
11. Leung CC, Yu IT, Chen W. Silicosis[J] Lancet. 2012;379(9830):2008–18.
12. Bonnard B, Ibarrola J, Lima-Posada I, et al. Neutrophil gelatinase-associated lipocalin from macrophages plays a critical role in renal fibrosis via the CCL5–Th2 cells–IL4 pathway[J]. Hypertension. 2021;79(2):352–64.
13. Galaris A, Fanidis D, Tsitoura E, et al. Increased lipocalin-2 expression in pulmonaryinflammation and fibrosis[J]. Front Med. 2023;10:1195501.
14. Zhang J, Yang X, Yang Y, et al. NF-κB mediates silica-induced pulmonary inflammation by promoting the release of IL-1β in macrophages[J]. Environ Toxicol. 2022;37(9):2235–43.

15. Oliver G, Kipnis J, Randolph GJ, et al. The Lymphatic Vasculature in the 21st Century: Novel Functional Roles in Homeostasis and Disease[J]. Cell. 2020;182(2):270–96.
16. Kuonqui K, Campbell AC, Sarker A, et al. Dysregulation of Lymphatic Endothelial VEGFR3 Signaling in Disease[J]. Cells. 2023;13(1):68.
17. Baluk P, Naikawadi RP, Kim S, et al. Lymphatic proliferation ameliorates pulmonary fibrosis after lung injury[J]. Am J Pathol. 2020;190(12):2355–75.
18. Cui J, He H, Xu H, et al. The regulatory effect of pulmonary lymphatic drainage on silicosis fibrosis[J]. Ecotoxicol Environ Saf. 2022;241:113758.
19. Chianese M, Screm G, Salton F, et al. Pirfenidone and Nintedanib in Pulmonary Fibrosis: Lights and Shadows[J]. Pharmaceuticals (Basel). 2024;17(6):709.
20. Wu Z, Yu B, He Q, et al. LCN2 drives ferroptosis-associated ischemia-reperfusion injury after renal transplantation: integrated machine learning and in vivo validation[J]. Apoptosis. 2025;30(11–12):3026–43.

Figures

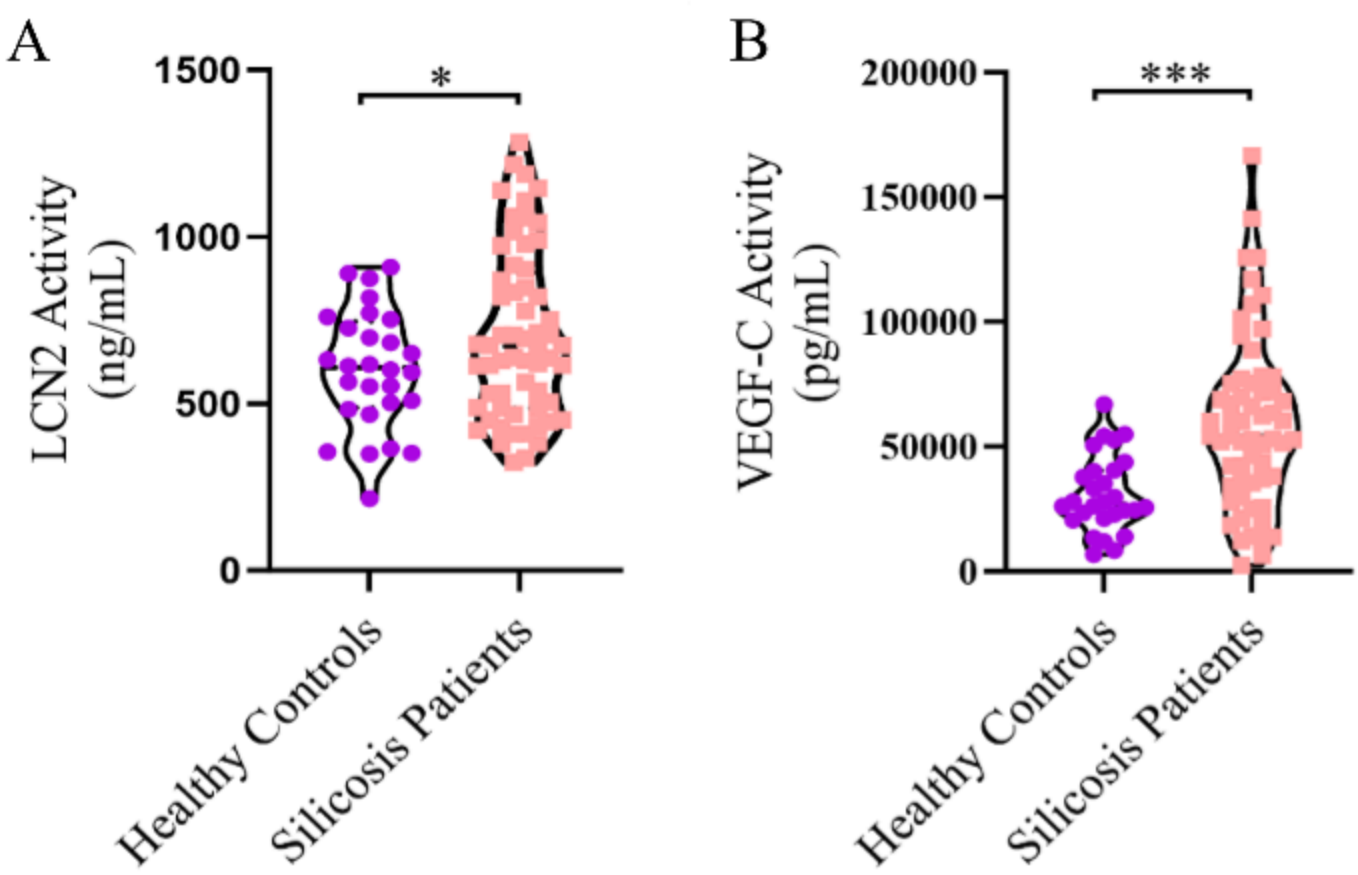


Figure 1

The levels of LCN2 and VEGF-C in the serum of silicosis patients were elevated. (A) Comparative analysis of serum LCN2 levels between healthy controls and silicosis patients. (B) Comparative analysis of serum VEGF-C levels between healthy controls and silicosis patients. *P < 0.05, ***P < 0.001.

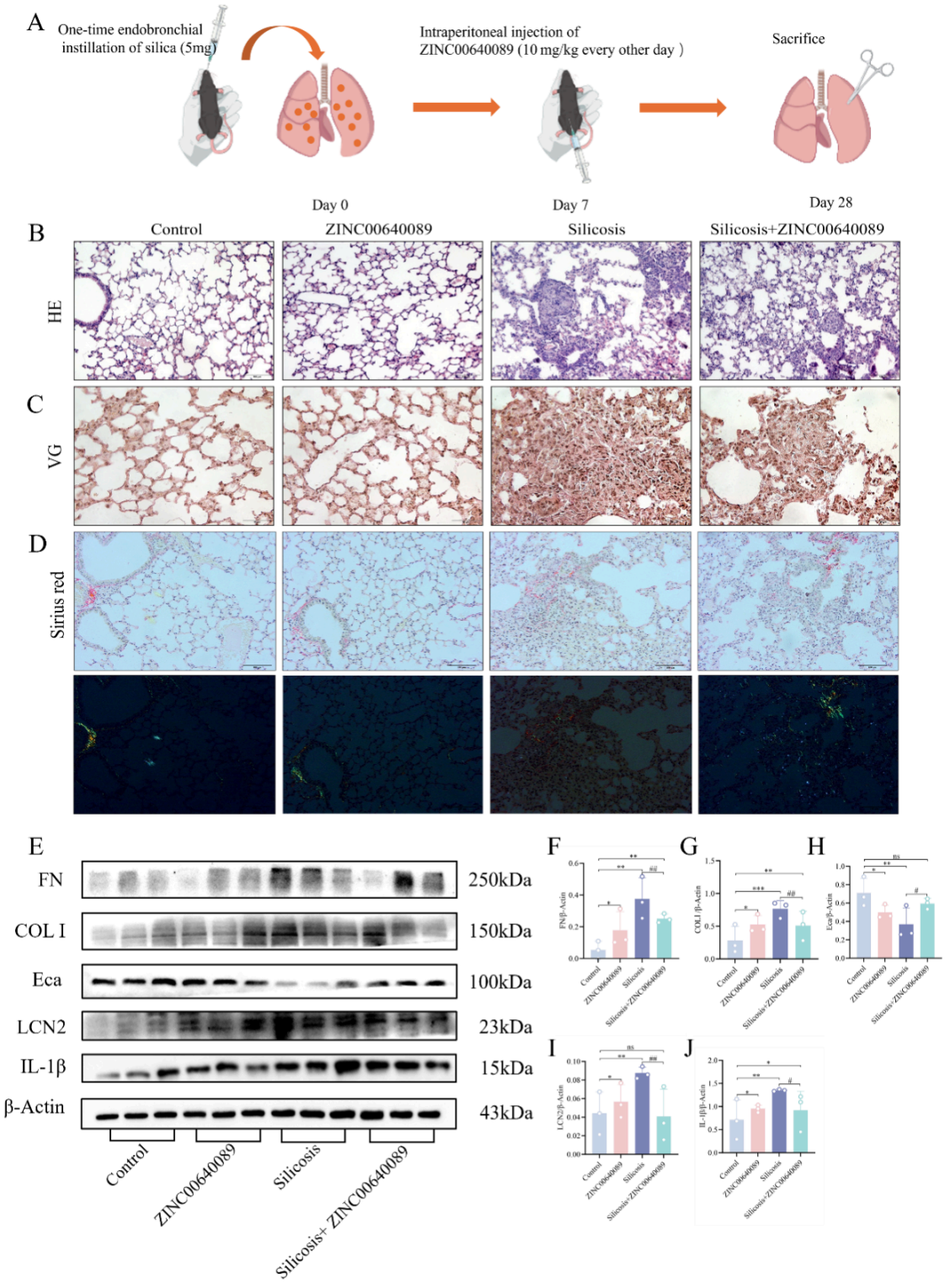


Figure 2

Targeted inhibition of LCN2 alleviates SiO_2-induced pulmonary fibrosis. (A) Schematic diagram of the treatment protocol using ZINC00640089 to inhibit LCN2 in a murine silicosis model. (B) HE staining. (C) VG staining. (D) Sirius red staining. (E–J) Western blot analysis of IL-1β, LCN2, COL1, FN, and Eca expression levels in lung tissue samples (n=3). compared with the Control group, *P < 0.05, **P < 0.01, ***P < 0.001; compared with the Silicosis group, $^{\#}P$<0.05, $^{\#\#}P$<0.01.

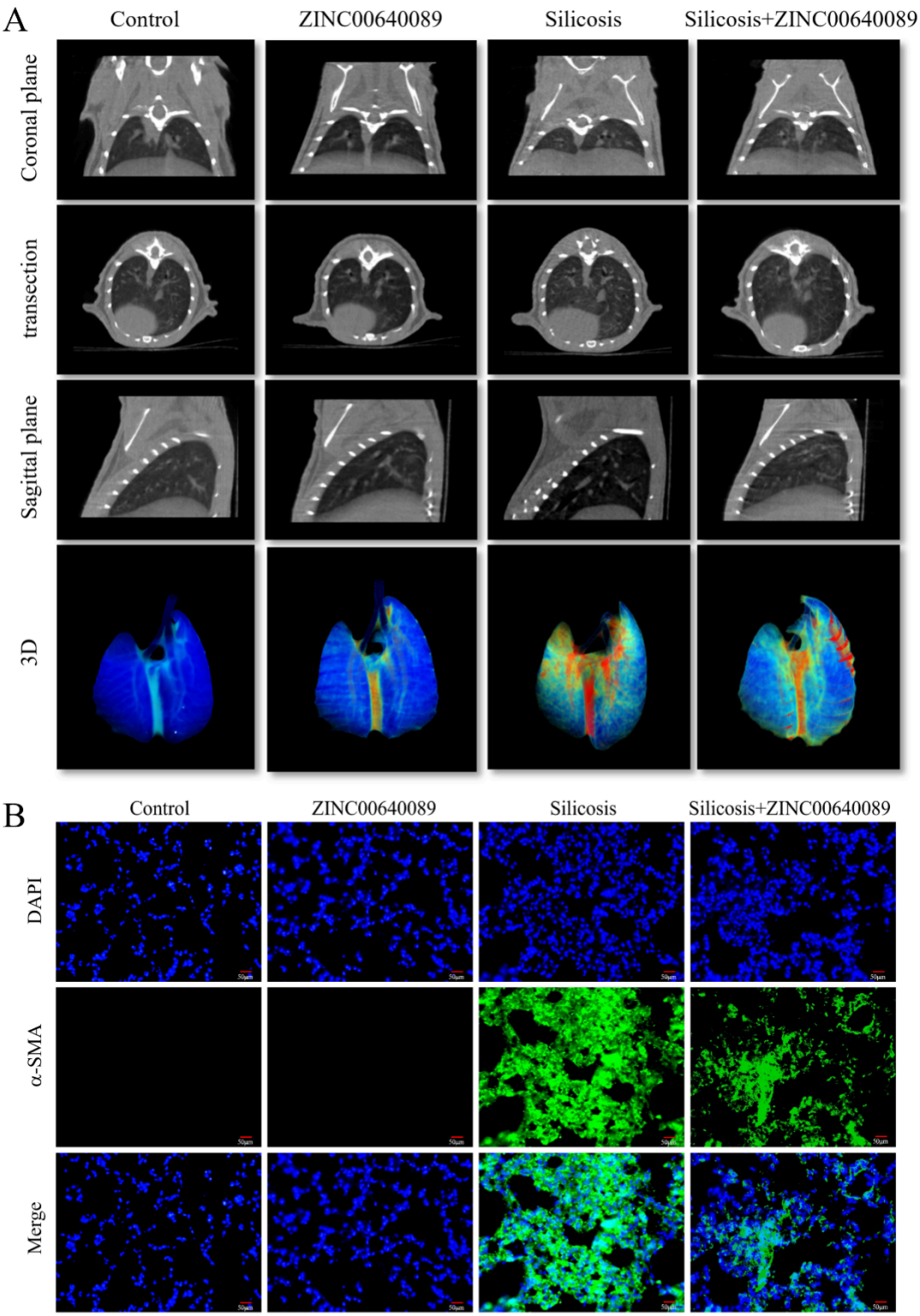


Figure 3

ZINC00640089 improves lung nodules and fibrosis levels in silicosis mice. (A) CT scan images of the coronal, transverse, and sagittal planes, as well as three-dimensional reconstructions of lungs from each group of mice. (B) Immunofluorescence staining of α-SMA in lung tissue sections.

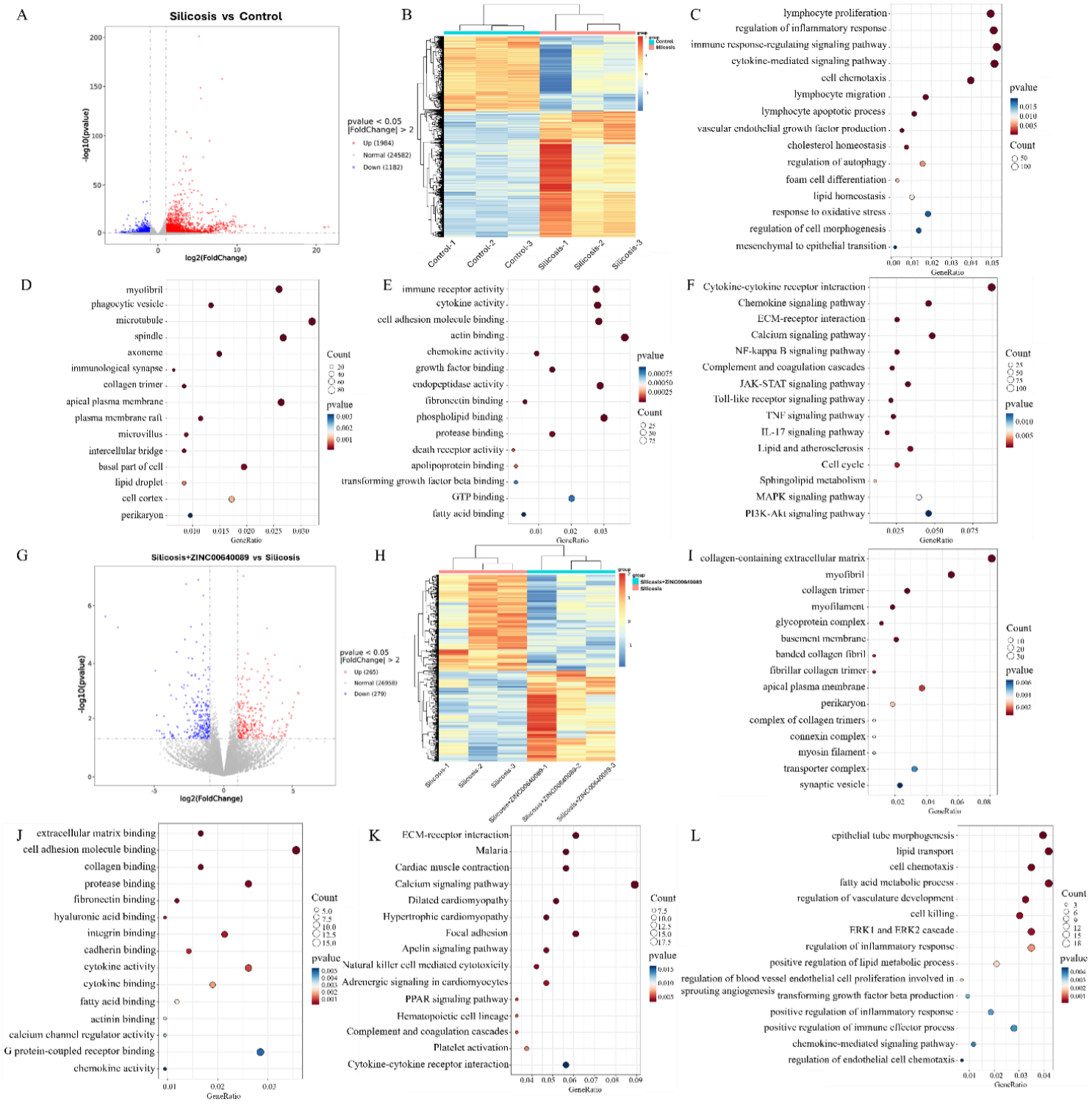


Figure 4

Transcriptomic analysis of ZINC00640089 intervention. (A) Volcano plot comparing Silicosis and Control groups. (B) Heatmap of hierarchical clustering analysis for differentially expressed genes between

Silicosis and Control groups. (C) Major biological processes enriched by differentially expressed genes in Silicosis versus Control groups. (D) Major cellular components enriched by differentially expressed genes in Silicosis versus Control groups. (E) Major molecular functions enriched by differentially expressed genes in Silicosis versus Control groups. (F) Major pathways enriched by differentially expressed genes in Silicosis versus Control groups. (G) Volcano plot comparing Silicosis+ZINC00640089 and Silicosis groups. (H) Heatmap of hierarchical clustering analysis for differentially expressed genes between Silicosis+ZINC00640089 and Silicosis groups. (I) Major biological processes enriched by differentially expressed genes in Silicosis+ZINC00640089 versus Silicosis groups. (J) Major cellular components enriched by differentially expressed genes in Silicosis+ZINC00640089 versus Silicosis groups. (K) Major molecular functions enriched by differentially expressed genes in Silicosis+ZINC00640089 versus Silicosis groups. (L) Major pathways enriched by differentially expressed genes in Silicosis+ZINC00640089 versus Silicosis groups.

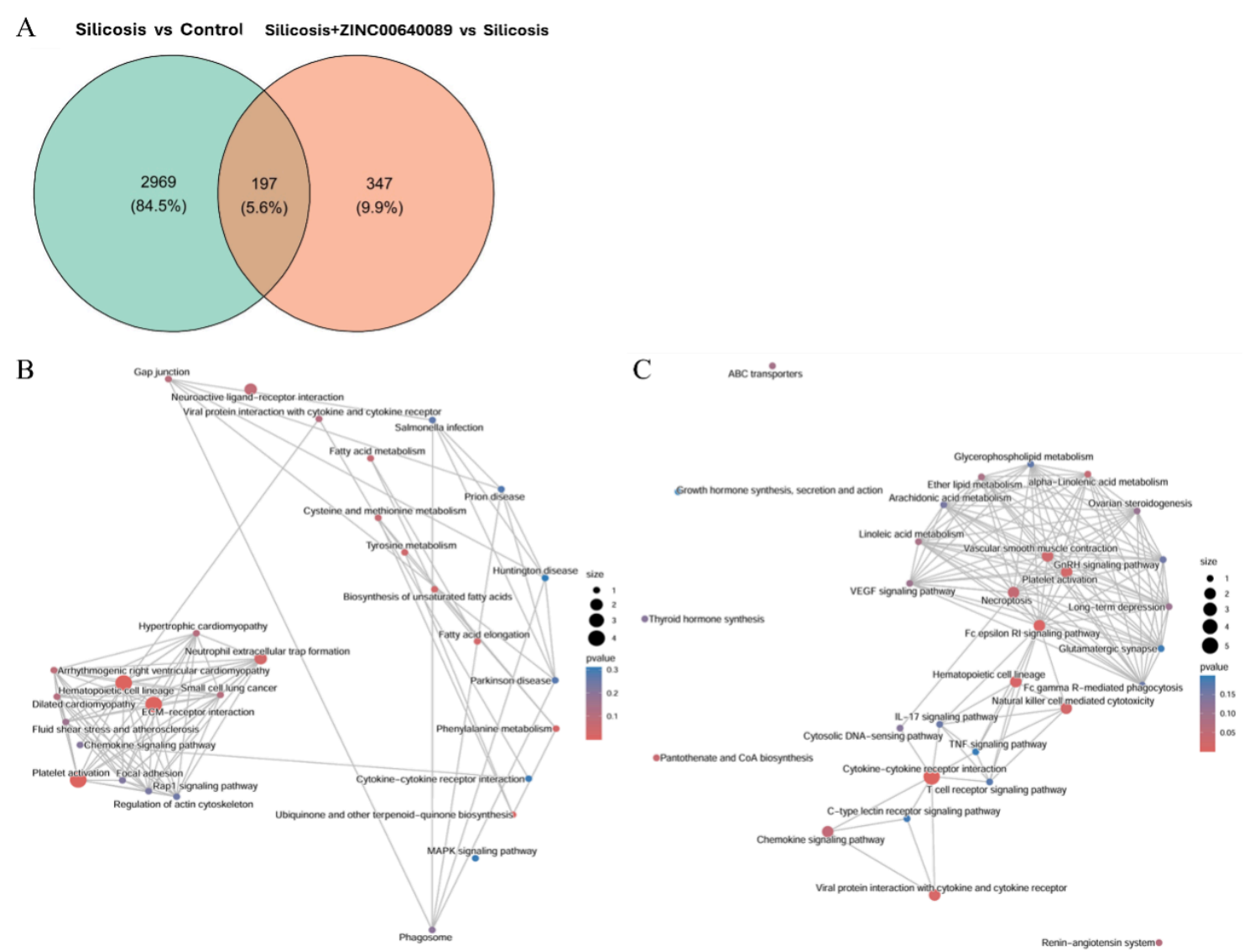


Figure 5

ZINC00640089 participates in regulating lymph-related signaling pathways in silicosis. (A) Venn diagram showing DEGs between the Silicosis group and Control group, and between the Silicosis+ZINC00640089 group and Silicosis group. (B) Network diagram of the top 30 significantly enriched KEGG pathways for genes upregulated in the Silicosis group but downregulated in the Silicosis+ZINC00640089 group. (C) Network diagram of the top 30 significantly enriched KEGG pathways for genes downregulated in the Silicosis group but upregulated in the Silicosis+ZINC00640089 group.

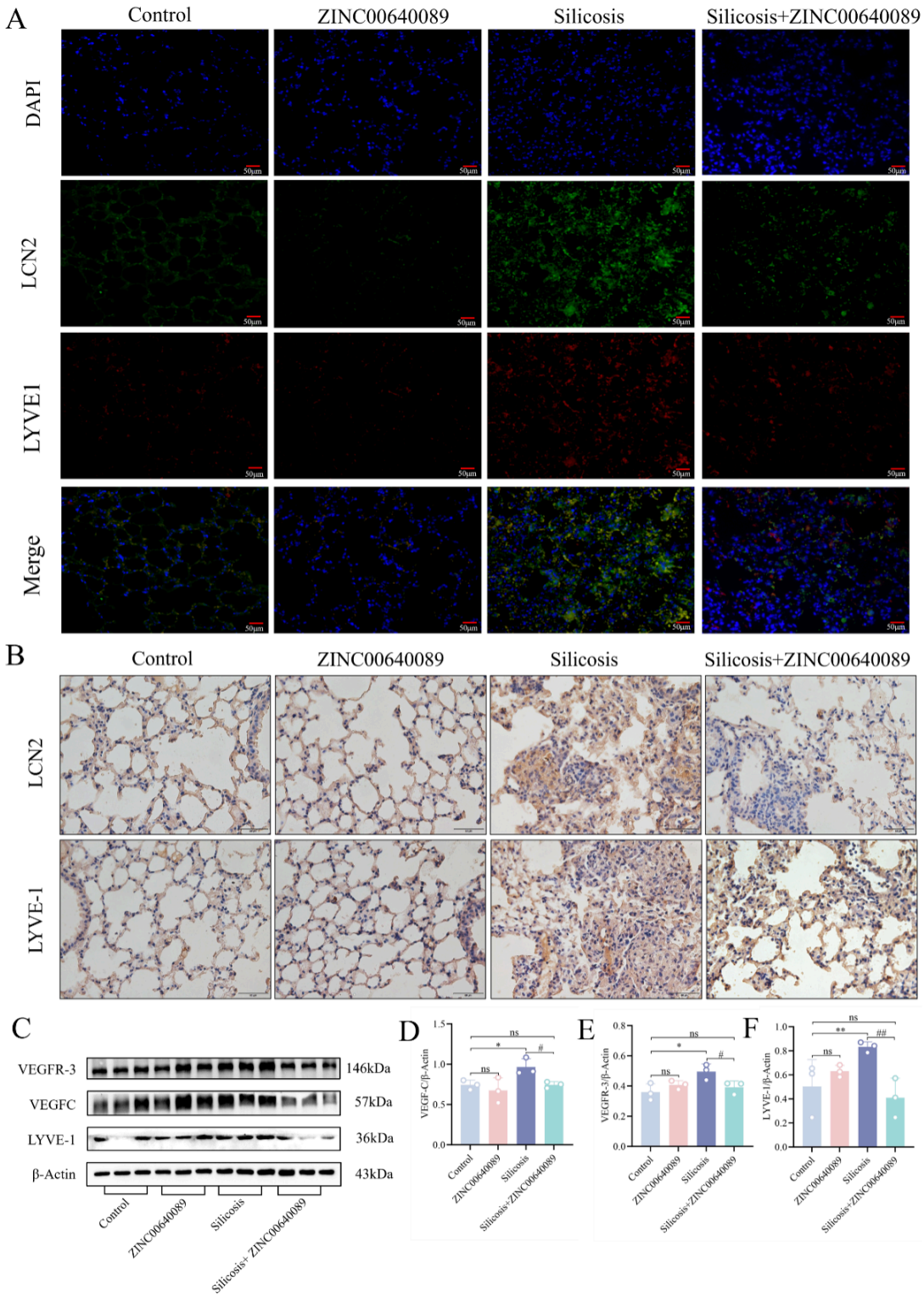


Figure 6

Inhibition of LCN2 blocked pathological lymphatic vessel formation. (A) Immunofluorescence colocalization analysis showing co-expression of LCN2 and LYVE-1 in lung tissue. (B) Immunohistochemical analysis of LCN2 and LYVE-1 expression in lung tissue. (C–G) Western blot analysis of VEGF-C, VEGFR-3, and LYVE-1 expression in lung tissue samples (n = 3). compared to the Control group, *$P < 0.05$, **$P < 0.01$; compared to the Silicosis group, $^{\#}P < 0.05$, $^{\#\#}P < 0.01$.

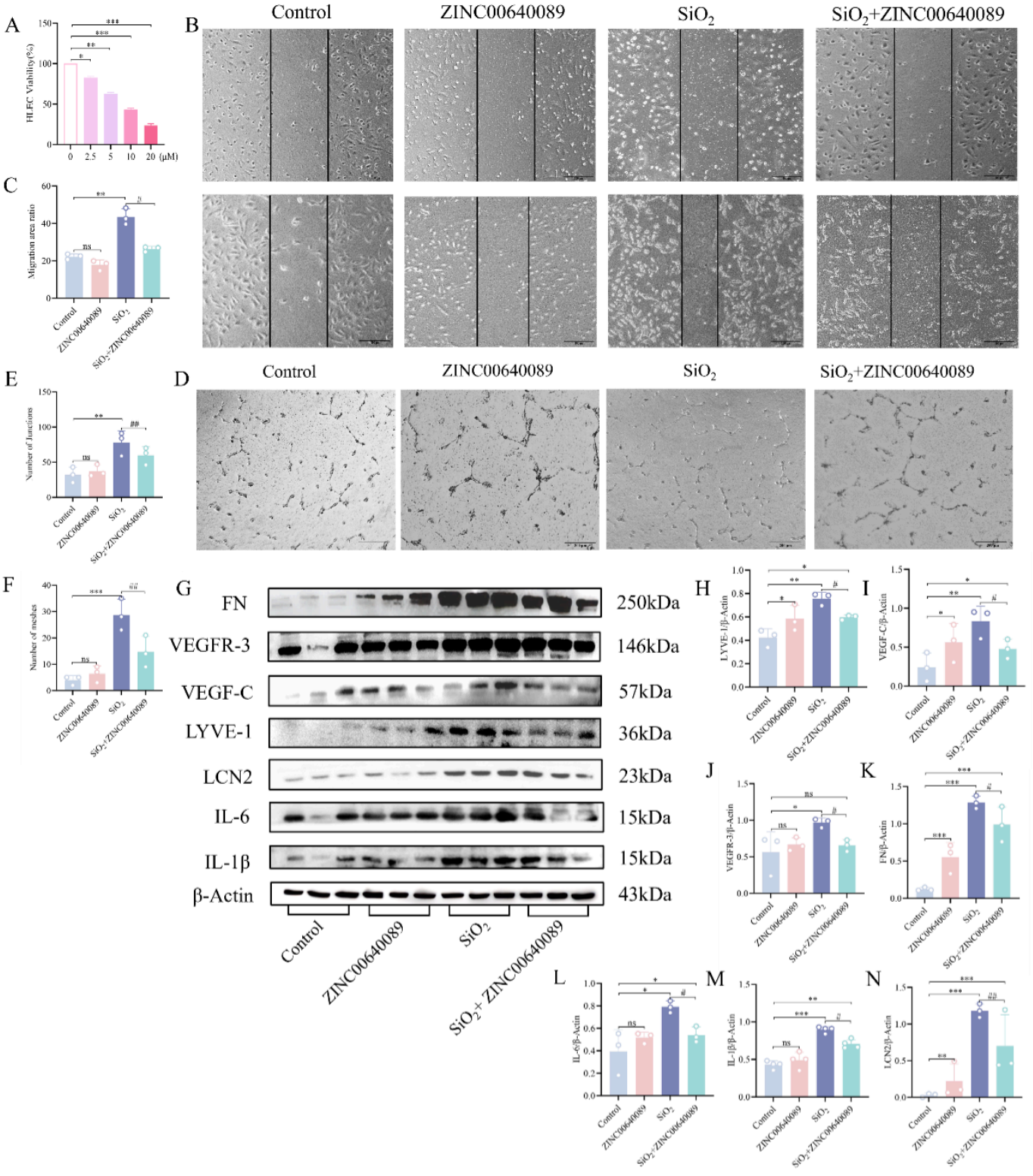


Figure 7

Targeted inhibition of LCN2 suppresses SiO_2-induced lymphatic vessel formation and inflammatory response in HLECs. (A) Cell viability of HLECs treated with different concentrations of the LCN2 inhibitor ZINC00640089 for 24 hours. (B-C) Scratch assays showed that ZINC00640089 inhibited SiO_2-enhanced cell migration within 24 hours. (D-F) Matrigel tube formation assays revealed that ZINC00640089 disrupted the dense tubular network structure induced by SiO_2, reducing total tube length, branch points, and lumen area. (G-N) Western blot analysis of protein expression levels of LCN2, LYVE-1, VEGF-C, VEGFR-3, FN, IL-6, and IL-1β (n=3). compared to the Control group, $^{*}P < 0.05$, $^{**}P < 0.01$, $^{***}P < 0.001$; compared to the SiO_2 group, $^{\#}P < 0.05$, $^{\#\#}P < 0.01$.

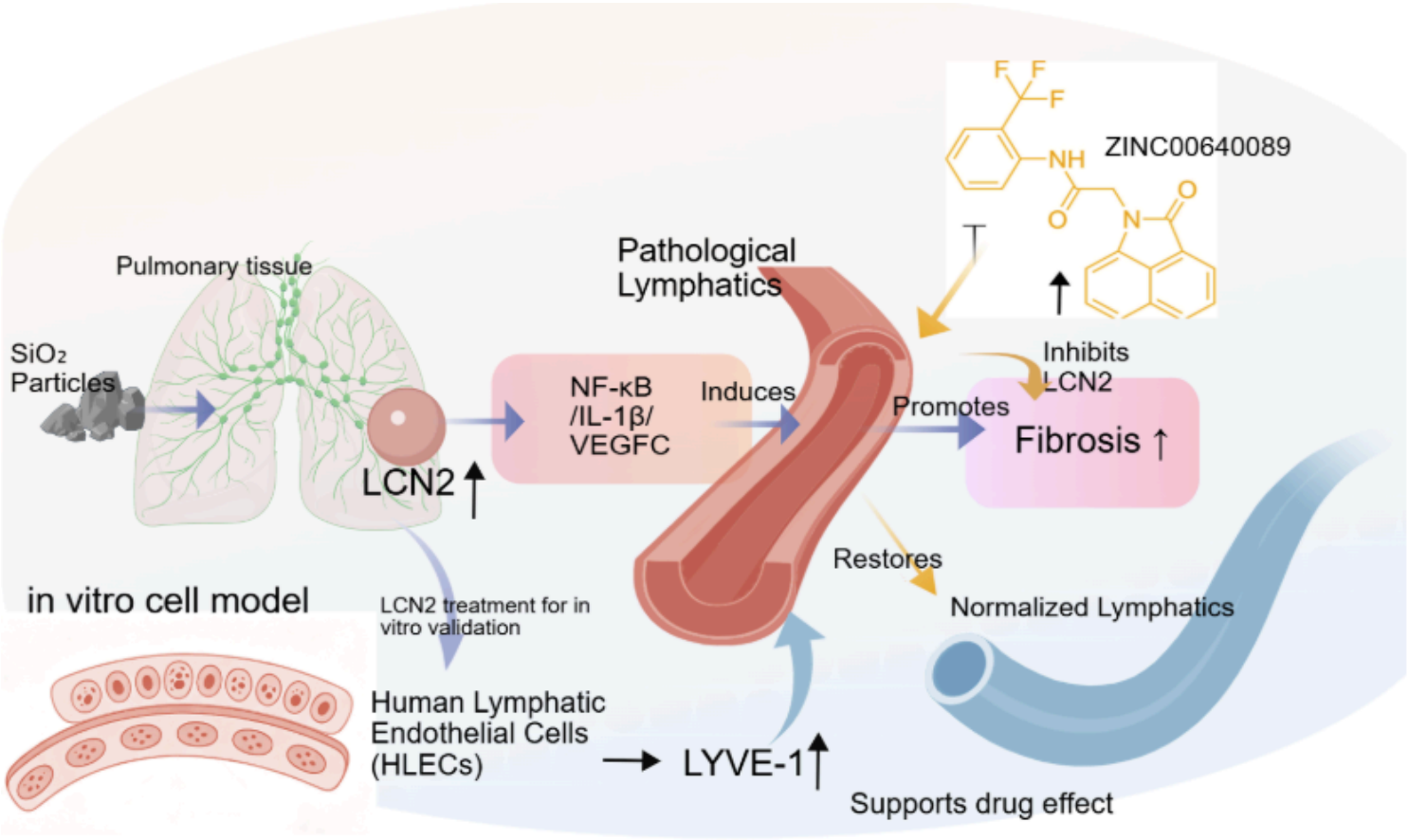


Figure 8

Targeted inhibition of LCN2 improves pathological lymphangiogenesis and fibrosis in silicosis